**PAPER • OPEN ACCESS**

# Extracting piezoresistive response of self-sensing cementitious composites under temperature effect via Bayesian blind source separation

To cite this article: Siqi Ding *et al* 2021 *Smart Mater. Struct.* **30** 065010

View the article online for updates and enhancements.

# Extracting piezoresistive response of self-sensing cementitious composites under temperature effect via Bayesian blind source separation

**Siqi Ding**[1,2] , **Chi Xu**[1,2], **Yi-Qing Ni**[1,2,*] and **Baoguo Han**[3]

[1] Department of Civil and Environmental Engineering, The Hong Kong Polytechnic University, Hung Hom, Kowloon, Hong Kong Special Administrative Region, People's Republic of China
[2] National Rail Transit Electrification and Automation Engineering Technology Research Center (Hong Kong Branch), Hung Hom, Kowloon, Hong Kong Special Administrative Region, People's Republic of China
[3] School of Civil Engineering, Dalian University of Technology, Dalian 116024, People's Republic of China

E-mail: ceyqni@polyu.edu.hk

## Abstract

Self-sensing cementitious composite (SSCC) has been viewed as a promising sensing technology for structural health monitoring and traffic detection on account of its high sensitivity, low cost, long-term stability and compatibility with concrete structures. However, temperature variation effects in the electrical resistance measurements would impede the potential application of SSCC. It is therefore of great significance to understand the temperature effects on the piezoresistive performance of SSCC and eliminate such effects. In this study, temperature effects on the electrical and piezoresistive properties of SSCCs with different contents of carbon nanotube/nano carbon black (CNT/NCB) composite fillers are investigated under varying temperatures ranging from $-20\,^\circ$C to $60\,^\circ$C and under concurrent temperature and loading variations. Experimental results show that an increase in CNT/NCB composite filler content can decrease the activation energy of SSCC and facilitate the transport of the charge carriers, thus attenuating the sensitivity of SSCC to temperature. Temperature variation has no effect on the piezoresistive repeatability of SSCC due to the stable overall distribution of conductive network in SSCC. However, temperature rise can reduce the piezoresistive sensitivity of SSCC. Aiming to diminish the effect of temperature on the piezoresistive property of SSCC, the SSCC responses to simultaneous temperature and loading excitations are then treated using a Bayesian blind source separation (BSS) method to reconstruct two independent sources.

---

* Author to whom any correspondence should be addressed.

Regardless of the CNT/NCB composite filler content, the reconstructed source in relation to temperature variation always has a high correlation with the measured temperature, indicating that the proposed Bayesian BSS method can well extract and separate the electrical resistance variation induced by temperature variation from that induced by simultaneous temperature and loading excitations.

## 1. Introduction

There are emerging trends that push the global community to develop smart infrastructure. The infrastructure is at the beginning of a digitally driven revolution. Structural health monitoring (SHM) that refers to monitoring changes in structural performance and providing real-time information about structural condition for safety assessment and maintenance scheduling is an important paradigm for infrastructure sustainability with smart digital insights [1–3]. As the core of an SHM system, highly sensitive, durable, accurate and low-cost sensors are desired to detect structural conditions in a long-term and sustainable manner. Up to now, a great number of sensing techniques with respect to different functions (vibration, displacement, strain, stress, temperature, etc) and mechanisms (electrical, electrochemical, optical, visual, acoustic, etc) have been developed and implemented in industrial applications [3–10]. Nevertheless, some sensory systems have drawbacks such as unsatisfactory performance in extreme environments, time-consuming and labor-intensive installation and maintenance, and incompatibility with the target structures which limit their scalable implementation and deployment on civil structures [11].

Recent advancement in smart materials opens new avenues to develop innovative sensing technologies for SHM applications. Self-sensing cementitious composite (SSCC), which is fabricated by adding conductive fillers (carbon-based or metallic materials) into conventional cementitious materials, has been considered as a promising supplement to the existing sensing technologies. The SSCC can transduce strain (or deformation), stress (or external force), temperature, and damage in itself into the variation of electrical signals. In particular, the ability of electrical resistance of SSCC changing with external force or induced strain, i.e. the pressure-sensitive property or piezoresistive property has been extensively explored. In comparison with conventional sensors, SSCC-engineered sensors have inherent host compatibility and an identical lifespan with the construction material due to its cementitious feature. In addition, owing to functional filler reinforcement, SSCC-engineered sensors exhibit remarkably enhanced mechanical properties and durability over conventional concrete [12–21]. The versatile, tunable, and easy-to-scale features of its fabrication process enable mediating SSCC-engineered sensors with controlled composition, dimension, and configuration to fulfill various engineering applications, such as strain sensing [22], damage localization [23], damage detection [24], structural modal identification [25], and traffic detection [26].

However, similar in behavior to a semiconductor, SSCC exhibits a negative temperature coefficient (NTC) of electrical resistivity, i.e. the resistivity decreases with increasing temperature [16, 27–30]. Wen *et al* [31] observed that the electrical resistivity of SSCC with carbon fibers (CFs) decreases when temperature increases from 0 °C to 45 °C and returns back in the cooling process. Sun *et al* [16] found that the temperature sensitivity of SSCC with multi-layer graphene (MLG) decreases with the increase of the volume fraction of MLG beyond the percolation threshold, which is consistent with the observation on SSCC with different volume fractions of CNT/NCBs [32] and CNT/CFs [33]. It is well known that tunneling conduction mechanisms play a dominant role in the electrical resistance change of SSCC under a temperature variation or loading variation condition [30]. Due to the coupling effect, it has been reported that the piezoresistive behavior of SSCC would be significantly affected by temperature [34–38]. Ou *et al* [37] found that temperature has a great influence on the fractional change in electrical resistance of SSCC with CF/CBs. They proposed a compensation circuit to eliminate the influence of temperature on the output of SSCC. Dong *et al* [38] observed that severe heat exchange between SSCC and its surrounding environments causes the output variation of SSCC under different temperatures, and that the piezoresistive properties including sensitivity and repeatability of SSCC are independent of temperature variation after applying a temperature compensation circuit similar to the work done by Ou *et al* [37] to remove the heat exchange interference. Whereas, Wang *et al* [34] and Monteiro *et al* [36] reported that the sensitivity of SSCC decreases with the temperature growth while the repeatability is not affected at temperatures ranging from −20 °C to 45 °C. The reduced sensitivity was explained as the enlarged distance between conductive fillers due to temperature increase, and thus the decreased tunneling current [34].

Temperature variation would be a major problem in application of SSCC to precisely detect strain/stress and damage, especially for long-term structural condition and health monitoring. In previous studies, only the temperature effect on piezoresistive properties of SSCC at stationary temperatures has been considered under static or dynamic loading. In practice, the temperature effect is usually time-varying in daily or yearly cycle [39]. The piezoresistive properties of SSCC under simultaneous temperature and loading variations have not been investigated. To remove the temperature-induced

output, the temperature compensation circuit based on subtracting the output of an additional unstressed SSCC from the output of the stressed SSCC has been proposed [37, 38]. However, this method requires additional apparatus and temperature information for calibration and is applicable only for specific SSCC, and is therefore inappropriate for scale-up applications. In addition, there are cases where temperature measurement is not available. In such situations, directly distinguishing temperature-induced change from the mixed structural response is a critical issue [40]. Several data normalization techniques have been used to remove the signal change caused by environmental variations in structural condition monitoring by means of impedance, vibration, and guided wave based methods [41–43]. However, no temperature extraction algorithm has been reported in dealing with the monitoring data collected by SSCC-engineered sensors in the presence of operational and environmental variations.

This paper, therefore, for the first time, pursues a Bayesian blind source separation (BSS) method to extract the temperature-induced resistance variation of SSCC under both temperature and loading excitations. This proposed method performs when the source signals such as temperature and loading are not observed and prior knowledge of the unknown sources is not available [44]. In the present study, the proposed method is coded in the MATLAB environment so that the temperature-induced resistance variation and the loading-induced resistance variation can be separated automatically during the continuous measurements [45]. To examine the effectiveness of the proposed Bayesian BSS method and understand the temperature influence mechanism, SSCCs with different contents of CNT/NCB composite fillers, which have demonstrated excellent piezoresistive sensitivity and repeatability [25, 46, 47], are fabricated and tested. The temperature effects on the electrical and piezoresistive properties of the SSCCs are then explored in consideration of temperatures ranging from −20 °C to 60 °C. Afterwards, the piezoresistive performance of the SSCCs under simultaneous temperature and loading variations is investigated. Lastly, the feasibility of the proposed method for extraction of the temperature-induced resistance variation from the mixed response of the SSCCs is verified.

## 2. Experimental materials and methods

### 2.1. Materials

The SSCCs were fabricated from cement, fly ash, water, superplasticizer and CNT/NCB composite fillers. The ASTM type I normal Portland cement 42.5R (Dalian Xiaoyetian Cement Co. Ltd, China) and fly ash (Dalian Huayuan Fly Ash Co. Ltd, China) were used as matrix materials. A polycarboxylate superplasticizer with a solid content of 45% (3310E, Sika Co. Ltd, China)was used to facilitate the workability of the mixtures. The commercially available CNT/NCB composite fillers from Chengdu Institute of Organic Chemistry Co. Ltd, China were employed as conductive fillers. The CNT/NCB composite fillers were synthesized via electrostatic self-assembly

**Table 1.** Physical properties of CNT/NCB composite fillers.

| Properties | Description/value |
|---|---|
| Mass ratio of CNTs/NCBs to hybrid (wt%) | 40/60 |
| Shape | Grape clusters |
| Specific gravity (g cm$^{-3}$) | 2.0 |
| Specific surface area (m$^2$ g$^{-1}$) | 65–75 |
| Electrical resistivity (Ω cm) | $10^{-3}$ |
| Outer diameter of CNTs (nm) | >50 |
| Length of CNTs ($\mu$m) | 10–20 |
| Specific surface area of CNTs (m$^2$ g$^{-1}$) | >40 |
| Tap density of CNTs (g cm$^{-3}$) | 0.18 |
| Particle size of NCBs (nm) | 23 |
| Specific surface area of NCBs (m$^2$ g$^{-1}$) | 125 |

technique. Table 1 summarizes the physical properties of the CNT/NCB composite fillers. The self-assembled hierarchical structure of the CNT/NCB composite fillers observed by a scanning electron microscope (SEM) (NanoSEM 450, FEI Ltd, USA) is illustrated in figure 1(a). The SEM image of the hardened SSCC sample with the CNT/NCB composite fillers is shown in figure 1(b). It is observed that the CNT/NCB composite fillers can be uniformly dispersed in cement matrix without using additional dispersion technique.

### 2.2. Specimen preparation

Our previous work has systematically investigated the electrical properties and self-sensing performance of SSCCs with different contents of CNT/NCB composite fillers and demonstrated that the percolation threshold zone of the SSCCs with CNT/NCB composite fillers is approximately within the range of 1 wt% ∼ 3 wt% [46]. Based on the previous work, the SSCC specimens in this study were fabricated according to the mix proportions listed in table 2. Figure 1(c) illustrates the preparation process of the SSCC specimens. First, polycarboxylate superplasticizer was added to water and stirred for 20 s in a beaker. Second, the pre-weighed cement and fly ash were poured into the aqueous solution at the same time and mixed using a mechanical stirrer (MXF-C, Shanghai Muxuan Industrial Co. Ltd, China) equipped with a 5 cm impeller propeller stirring blade at a speed of 400 rpm for 2 min. Third, the CNT/NCB composite fillers were gradually added to the mixture and mechanically mixed at a speed of 400 rpm for 3 min, applying no additional dispersion technique. Fourth, the resulting mixture was evenly poured into a 20 mm × 20 mm × 40 mm rectangle oiled mold. Two copper electrodes with openings of 2 mm × 2 mm were then embedded in the middle of each specimen with an interval of 20 mm. Subsequently, the specimens were vibrated for 10 s to eliminate bubbles using an electric vibrator before placing into curing chamber for 1 d. Lastly, after demolding, the specimens were cured in a water bath at 20 °C for 28 d. Since C–S–H gel in pastes cured at 60 °C tends to collapse towards a denser material with fewer large gel pores, all the specimens were dried in a vacuum oven at 50 °C for 5 d prior to test in order to
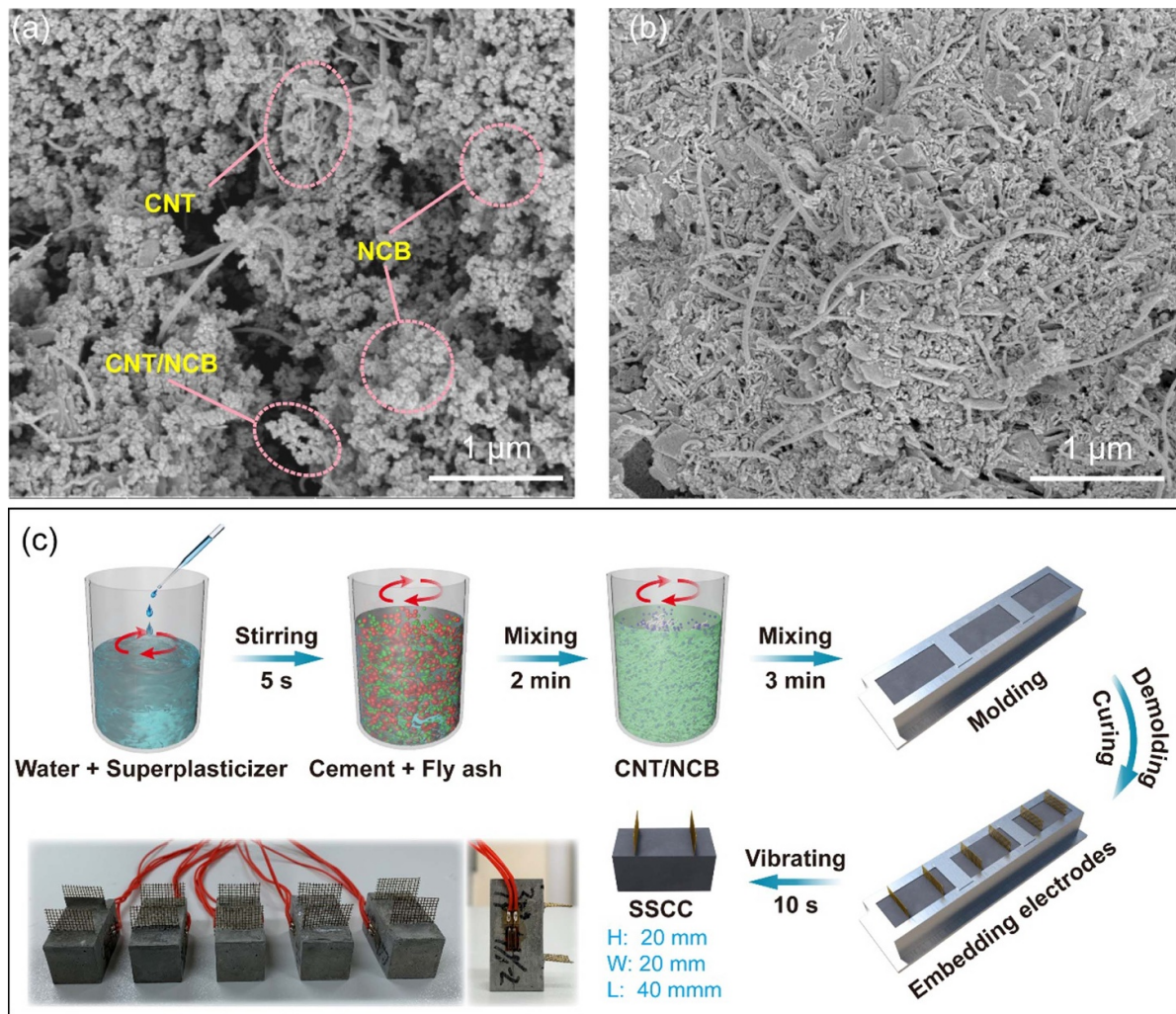
**Figure 1.** (a) SEM image of CNT/NCB composite fillers. (b) CNT/NCB composite fillers uniformly distributed in cement matrix forming extensive conductive network. (c) Schematic diagram of preparation process of SSCCs with CNT/NCB composite fillers.

**Table 2.** Mix proportions of SSCCs with CNT/NCB fillers.

| No. | Cement | CNT/NCB | Water | Fly ash | Superplasticizer |
|---|---|---|---|---|---|
| SSCC-0 | 1 | 0 | 0.2 | 0.15 | 1.5% |
| SSCC-1 | 1 | 0.01 | 0.2 | 0.15 | 1.5% |
| SSCC-3 | 1 | 0.03 | 0.2 | 0.15 | 1.5% |
| SSCC-5 | 1 | 0.05 | 0.2 | 0.15 | 1.5% |
| SSCC-10 | 1 | 0.1 | 0.2 | 0.15 | 1.5% |
| SSCC-15 | 1 | 0.15 | 0.2 | 0.15 | 1.5% |

Note: The amount of CNT/NCB, water, fly ash, and superplasticizer is by mass of cement.

minimize the effect of water content variation on the electrical and self-sensing properties while maintaining the structural integrity of SSCCs [48].

## 2.3. Experiment

*2.3.1. Tests on temperature effects.* In order to evaluate the temperature-sensitive property of the SSCCs, the temperature sensitivity ($|\text{FCR}|/\Delta T$, here $\Delta T$ is temperature variation and FCR is the fractional change in electrical resistance) of the

SSCCs was assessed by placing each specimen into an environmental chamber (GDJS-100, Linpin Instrument, China) and subjecting it to temperature variation from $-20\,°C$ to $60\,°C$ at intervals of $10\,°C$. The temperature range was determined based on service temperatures commonly suffered by concrete structures while maintaining the integrity. At each temperature considered, the specimen was insulated for 1 h to ensure external and internal temperature equilibrium. The DC electrical resistance was then measured by the two-probe method using a digital multimeter (DMM7510, Keithley Instruments
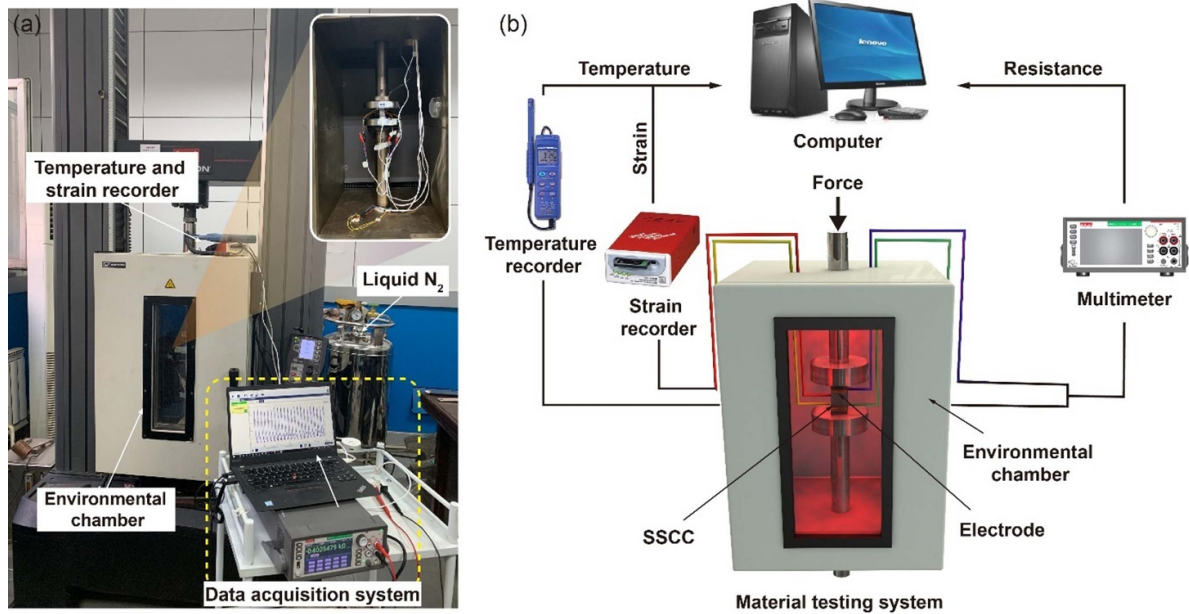
**Figure 2.** (a) Photo and (b) schematic diagram of experimental set-up for piezoresistive property tests of the SSCCs under different temperatures.

Inc., USA). For each specimen, the electrical resistance was taken the average of five repeated measurements. For cyclic heating-cooling tests, the environmental chamber was continuously operated, and the DC electrical resistance was continuously collected in each heating-up and cooling-down cycle. Meanwhile, a thermocouple connected with a digital temperature meter (HH310, Omega Engineering Inc., USA) was mounted on the surface of each specimen for calibration during each measurement.

*2.3.2. Piezoresistive property under constant temperatures.* In order to evaluate the piezoresistive property of the SSCCs, the FCR was monitored during compression:

$$\text{FCR} = \frac{\Delta R}{R_0} = \frac{R_t - R_0}{R_0} \tag{1}$$

where $\Delta R$ is the change in electrical resistance, $R_0$ and $R_t$ are the measured electrical resistances prior to loading and at time $t$, respectively. In order to guarantee elastic deformation of the SSCCs, the piezoresistive property of the SSCCs under constant temperatures was obtained by repeated compression tests with a stress amplitude of 10 MPa and a constant loading rate of 0.6 mm min$^{-1}$ using a universal mechanical testing machine (Instron 5982, Instron Inc., USA) equipped with an environmental chamber (3119-610, Instron Inc., USA). The environmental chamber equipped with a liquid N$_2$ cooling module can achieve a minimum temperature of $-150\,^\circ$C. The temperatures of $-20\,^\circ$C, $0\,^\circ$C, $20\,^\circ$C, $40\,^\circ$C and $60\,^\circ$C were addressed to investigate the effect of temperature on the piezoresistive property. Similarly, prior to imposing loading, the specimen was insulated for 1 h to reach temperature equilibrium at each temperature setting.

Afterwards, the DC electrical resistance was measured using the DMM7510 digital multimeter. In addition, two longitudinal strain gauges were symmetrically deployed on the opposite sides of the specimen and a dynamic data logger (DC-204R, Sokki Kenkyujo Co. Ltd, Japan) was used for strain measurement.

*2.3.3. Piezoresistive property under alternating temperatures.* In order to evaluate the piezoresistive property of the SSCCs under alternating temperatures, cyclic compression with a stress amplitude of 10 MPa and a constant loading rate of 0.6 mm min$^{-1}$ was continuously applied. Meanwhile, the specimen for test was cooled to a certain temperature for 1 h and then heated under the control of environment chamber. During the heating process, quick and slow opening/closing of the chamber door was exerted to simulate quick and slow temperature variations. The alternating temperature was recorded using the HH310 digital temperature meter with a sampling frequency of 1 Hz. In this experiment, signals including strain, electrical resistance, and force were collected simultaneously with a sampling frequency of 10 Hz. The experimental set-up is shown in figure 2.

## 3. Results and discussion

### 3.1. Temperature-sensitive property of SSCCs with CNT/NCB

Figure 3 shows the temperature dependence of electrical resistance of the SSCCs with different contents of CNT/NCB composite fillers in the range of temperature from $-20\,^\circ$C to $60\,^\circ$C. It can be seen that the electrical resistances of the SSCCs with and without CNT/NCB composite fillers all exhibit inverse trends with increasing temperature, namely NTC effect, which is a typical behavior of semiconductor [49].
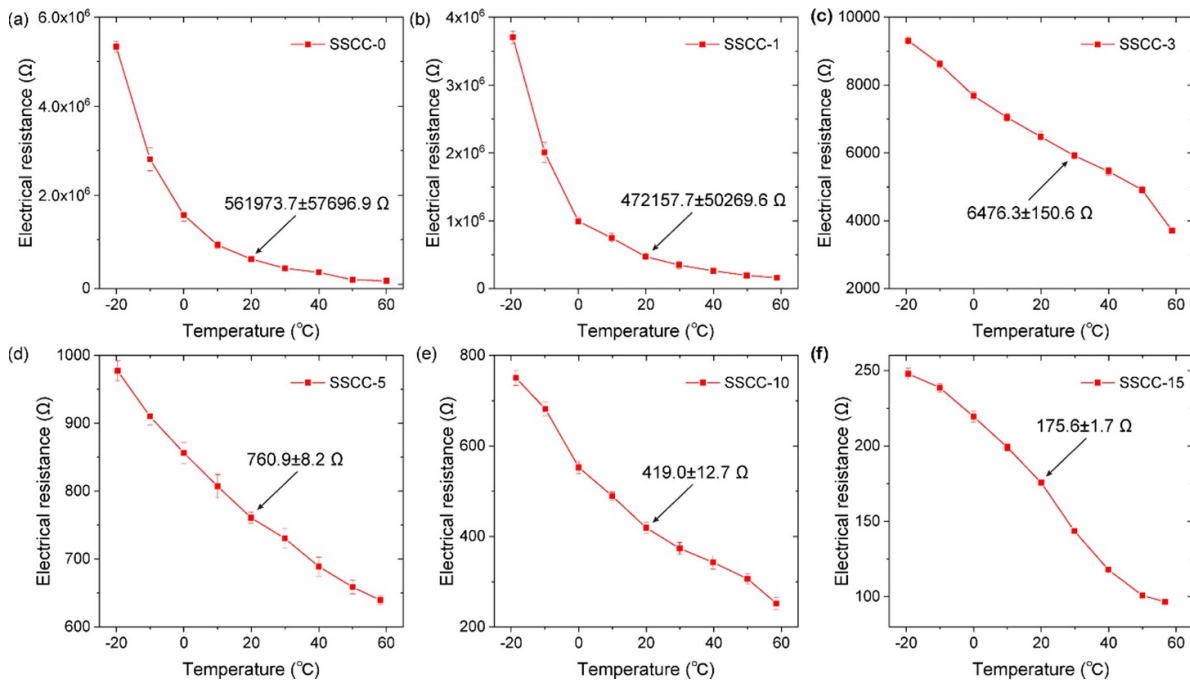
**Figure 3.** Temperature dependence of electrical resistance of SSCCs with CNT/NCB composite fillers. (a) SSCC-0. (b) SSCC-1. (c) SSCC-3. (d) SSCC-5. (e) SSCC-10. (f) SSCC-15. The electrical resistance of each SSCC at 20 °C is specified.

The NTC effect is in general observed in the SSCCs with various conductive fillers such as CF, MLG, CNT, and steel fiber [16, 31, 50].

To more clearly illustrate the temperature-sensitive property of the SSCCs with and without CNT/NCB composite fillers, the relationship between the FCR of the SSCCs with CNT/NCB composite fillers and temperature is shown in figure 4(a). The FCR shows the maximum value in the case of the control sample (i.e. the specimen SSCC-0), which is 96.21% in the full temperature range. The specimen SSCC-1 has almost the same temperature-sensitive behavior as the control sample and a similar FCR of 95.70%. This phenomenon indicates that 1.0 wt% CNT/NCBs in the cementitious composites is too low to form extensive conductive network. With increasing filler content, the FCR tends to decrease first and reaches the lowest value 34.57% in the case of 60 °C which is associated with the specimen SSCC-5, and then increase to 66.40% for the specimen SSCC-10 and 61.01% for the specimen SSCC-15 at the same temperature. The dependence of temperature-sensitive behavior of the SSCCs on filler content agrees well with their percolation behavior. Figure 4(b) shows the electrical resistances of the SSCCs as a function of filler content. A rapid decrease in the electrical resistance, i.e. percolation of the SSCCs, takes place when the filler content is above 1.0 wt%, forming a percolation zone marked in orange in figure 4(b). The result is consistent with our previous studies [32, 46]. It should be noticed that the effect of temperature on the percolation behavior of the SSCCs is much less than the effect of filler content. As shown in figure 4(b), the percolation curves at different temperatures remain almost unchanged.

The temperature sensitivity of electrical resistance of an SSCC is contingent on its filler content, which is attributed to different electrical conduction mechanisms governed by filler contents [30]. In general, temperature induces a change in electrical resistance of an SSCC in three ways: (a) thermally induced volume change of the SSCC including cement matrix and conductive fillers. The expansion or contraction of the SSCC leads to an increase or decrease of electrical resistance due to variation in potential barrier width of CNT/NCB composite fillers [34]. However, the volume change of the SSCC due to temperature variation is very small and can be neglected at temperatures lower than 60 °C. A temperature higher than 150 °C can lead to structural breakage and thermal expansion of the hydrated cement paste, and thus a positive temperature coefficient of electrical resistivity [28]. This case is not considered in this study; (b) thermally induced change of intrinsic electrical conductivity of CNT/NCB composite fillers. This can also be ignored due to the extremely high electrical conductivity of CNT/NCB composite fillers; (c) thermal-activated motion of charge carriers. In an SSCC, electrical conduction is brought about by the accumulation of charge carrier movements (electrons and holes mainly from CNT/NCB composite fillers and ions from capillary pore water and crystalline water in cement paste). The mobility of the charge carriers is temperature activated, while the concentration of charge carriers is solely determined by filler content, i.e. temperature independent. The dependence of electrical conductivity on temperature can be described by the Arrhenius equation [51],

$$\delta = A \exp\left(-\frac{E_a}{k_B T}\right) \qquad (2)$$
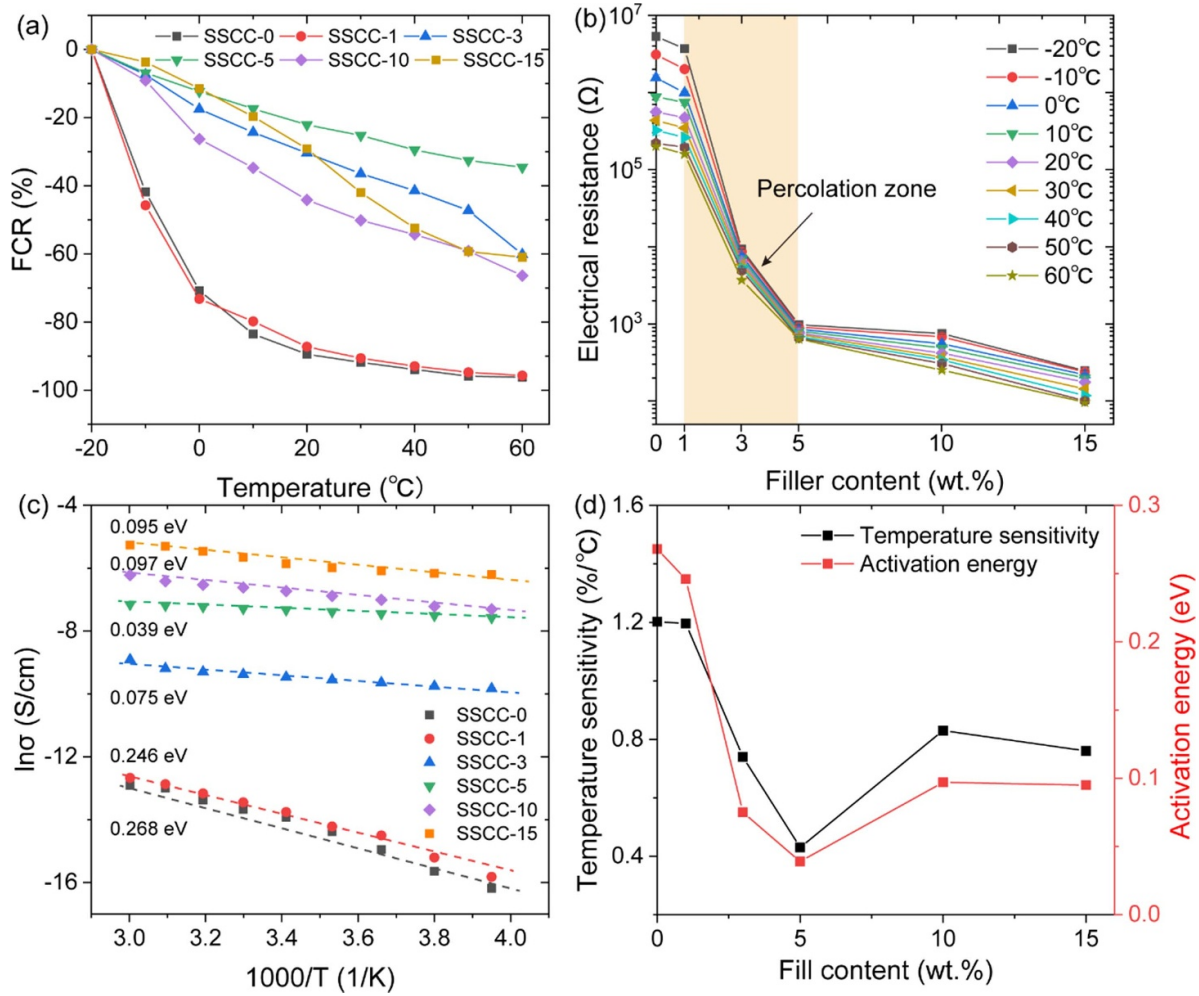
**Figure 4.** (a) FCR of SSCCs with CNT/NCB composite fillers as a function of temperature. (b) Electrical resistance of SSCCs as a function of filler content under different temperatures. (c) Arrhenius plots of electrical conductivity versus reciprocal absolute temperature for SSCCs with CNT/NCB composite fillers. (d) Temperature sensitivity and activation energy of SSCCs with CNT/NCB composite fillers as a function of filler content.

where $\delta$ is the electrical conductivity of the SSCC, $k_B$ is the Boltzmann constant ($8.6174 \times 10^{-5}$ eV K$^{-1}$), $A$ is a pre-exponential constant, $T$ is the absolute temperature, and $E_a$ is the activation energy for electrical conduction.

Figure 4(c) shows the Arrhenius plots of electrical conductivity versus the reciprocal of absolute temperature for the SSCCs with and without CNT/NCB composite fillers. The $E_a$ for each SSCC specimen can be determined from the slopes of the Arrhenius plots, as shown figure 4(c). The specimen SSCC-0 has the highest $E_a$ of 0.268 eV, which is close to the value of the specimen SSCC-1 (0.246 eV). When the filler content is increased to 5 wt%, the activation energy of the SSCC declines sharply to the lowest, 0.039 eV. This indicates that the CNT/NCB composite fillers can diminish the activation energy of the SSCCs and facilitate the transport of the charge carriers. This is because of the higher activation energy required for electrical conduction in semi-conductive cement matrix than that in conductive CNT/NCB composite fillers [51]. However, further increase of the filler content gives only a slight increase in activation energy of the SSCCs, which may be ascribed to the metal-like behavior of the SSCCs at

high filler doping when the concentration of charge carriers is high and the scattering of charge carriers and electron–phonon collisions generated with increasing temperature hinders the mobility of charge carriers [52].

The temperature sensitivity of each SSCC specimen is also presented in figure 4(d) for comparison. Interestingly, it is observed that the temperature sensitivity of the SSCCs with different filler contents has an identical change trend with the activation energy, indicating that the SSCCs with high activation energy demonstrate high temperature sensitivity. This phenomenon can be explained from the perspective of the formation of conductive network as a function of filler content. In the percolation zone, the tunneling conduction of charge carriers is always dominant. The tunneling current as a function of temperature can be expressed as [53]:

$$J = \frac{c_1}{d^2} e^{\left(-c_0 d - \frac{E_a}{k_B T}\right)} \tag{3}$$

where $c_0 = 4\pi\sqrt{2m\lambda}/h$, $c_1 = \lambda B V e^2/h \sin \pi B k_B T$, $B = 2\pi A/h\sqrt{2m\lambda}$, $d$ is the tunneling gap, $E_a$ is the activation
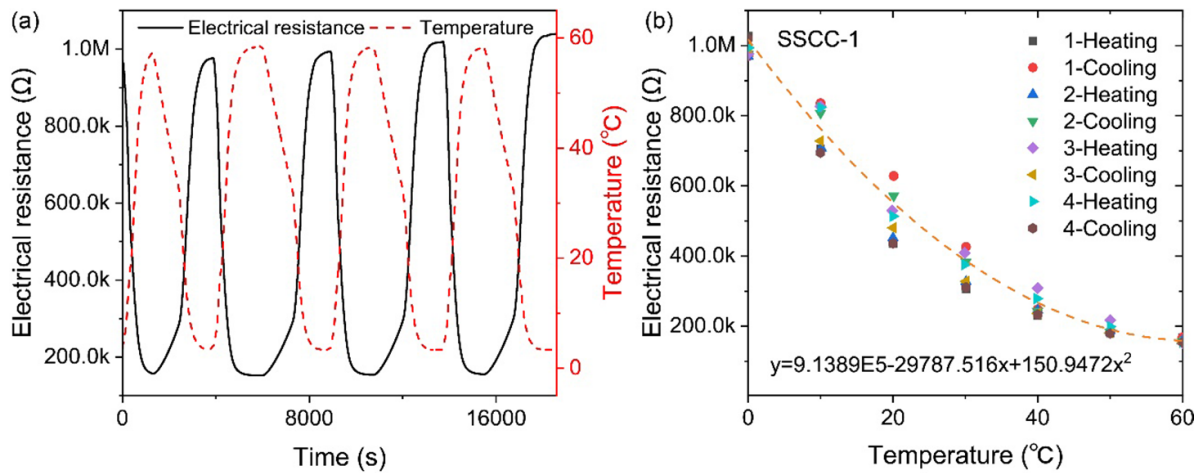
7

**Figure 5.** Temperature-sensitive property of SSCC-1 during four heating-cooling cycles.
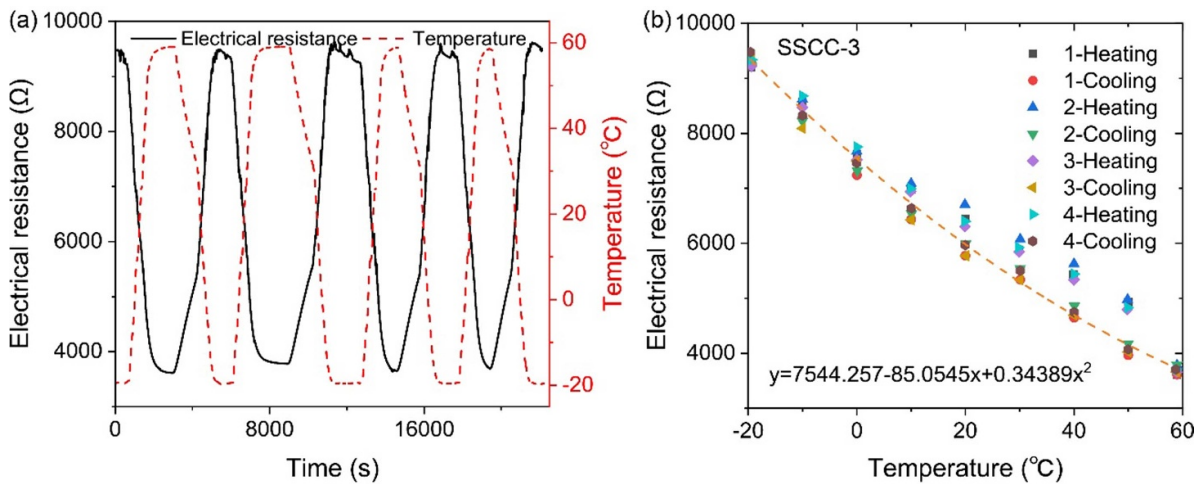


**Figure 6.** Temperature-sensitive property of SSCC-3 during four heating–cooling cycles.

energy, $k_{\mathrm{B}}$ is the Boltzmann constant, $T$ is the absolute temperature, $m$ is the electron mass, $\lambda$ is the average potential barrier, $h$ is the Planck constant, $V$ is the tunneling voltage, $e$ is the electron charge, and $A$ is a constant. It is seen that an increase in temperature makes a significant increase in the tunneling current, and thus decreases the electrical resistance. In addition, since the change of electrical resistance in the percolation zone is extremely sensitive to external effects such as temperature, stress, and filler content, an increase in temperature leads to a thermal fluctuation induced percolation of the conductive network, i.e. a high temperature sensitivity [54]. When the filler content is above the percolation threshold, extensive conduction paths are formed throughout the matrix, in which conduction through the conductive fillers in contact dominates. At this stage, the formation of conductive network is not sensitive to temperature variation, thus attenuating the temperature sensitivity.

The repeatability of the temperature-sensitive property of the SSCCs with CNT/NCB composite fillers is also investigated by conducting four heating–cooling cycles ranging from −20 °C to 60 °C as shown in figures 5–9. For brevity, the

case of the specimen SSCC-0 is neglected due to its similar temperature-sensitive property with the specimen SSCC-1. Since the SSCC samples were dried at 50 °C for 5 d prior to test, unbound or non-crystalline water in cement capillary pores is largely removed and the electrical polarization induced by ionic conduction is not observed for all the SSCC specimens [55]. In all the tests, the electrical resistance is gradually reduced upon heating and successively increased upon cooling. The lowest and highest electrical resistance values from the different cycles remain almost the same, indicating good repeatability of the temperature-sensitive property of the SSCCs.

Figures 5(b)–9(b) show the cyclic temperature–electrical resistance curves of the SSCCs, which display indistinct hysteresis loops in the forward and backward curves, implying high repeatability of temperature response of the SSCCs. In addition, there are quite good polynomial fitting (polyfit) results of the electrical resistance versus temperature. This excellent temperature-sensitive property of SSCCs suggests the possibility of SSCCs to serve as temperature sensors.
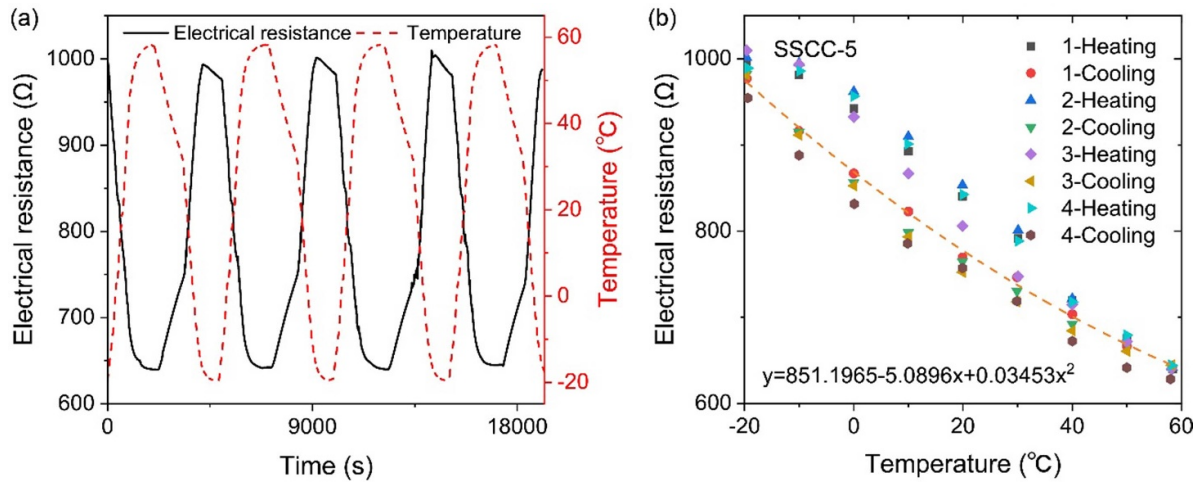
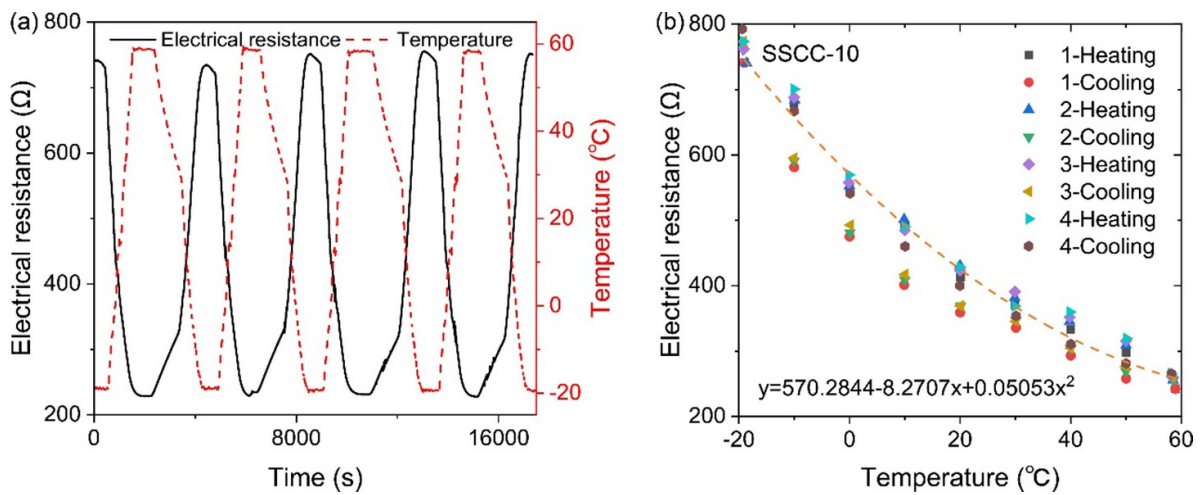**Figure 7.** Temperature-sensitive property of SSCC-5 during four heating–cooling cycles.



**Figure 8.** Temperature-sensitive property of SSCC-10 during four heating–cooling cycles.
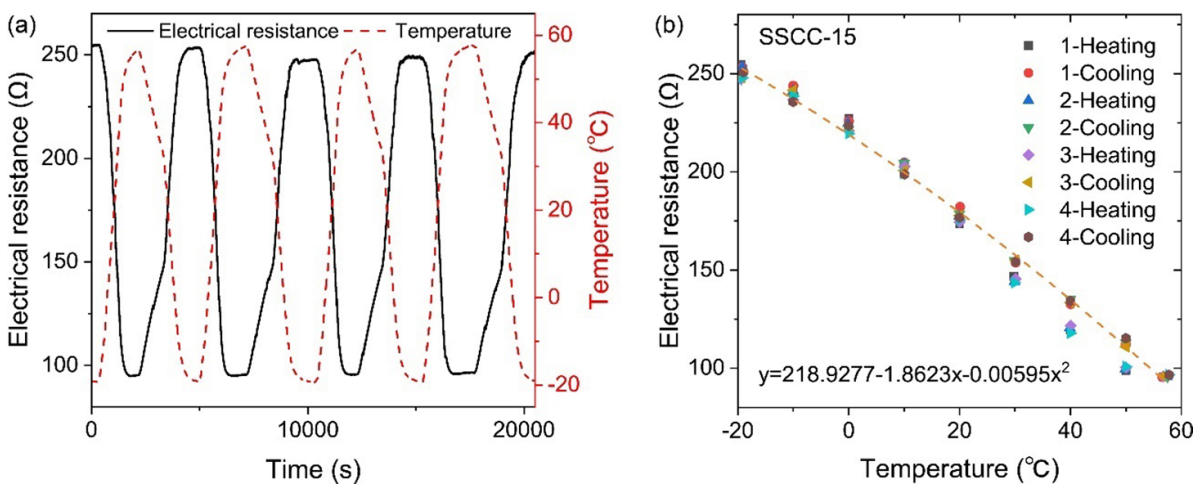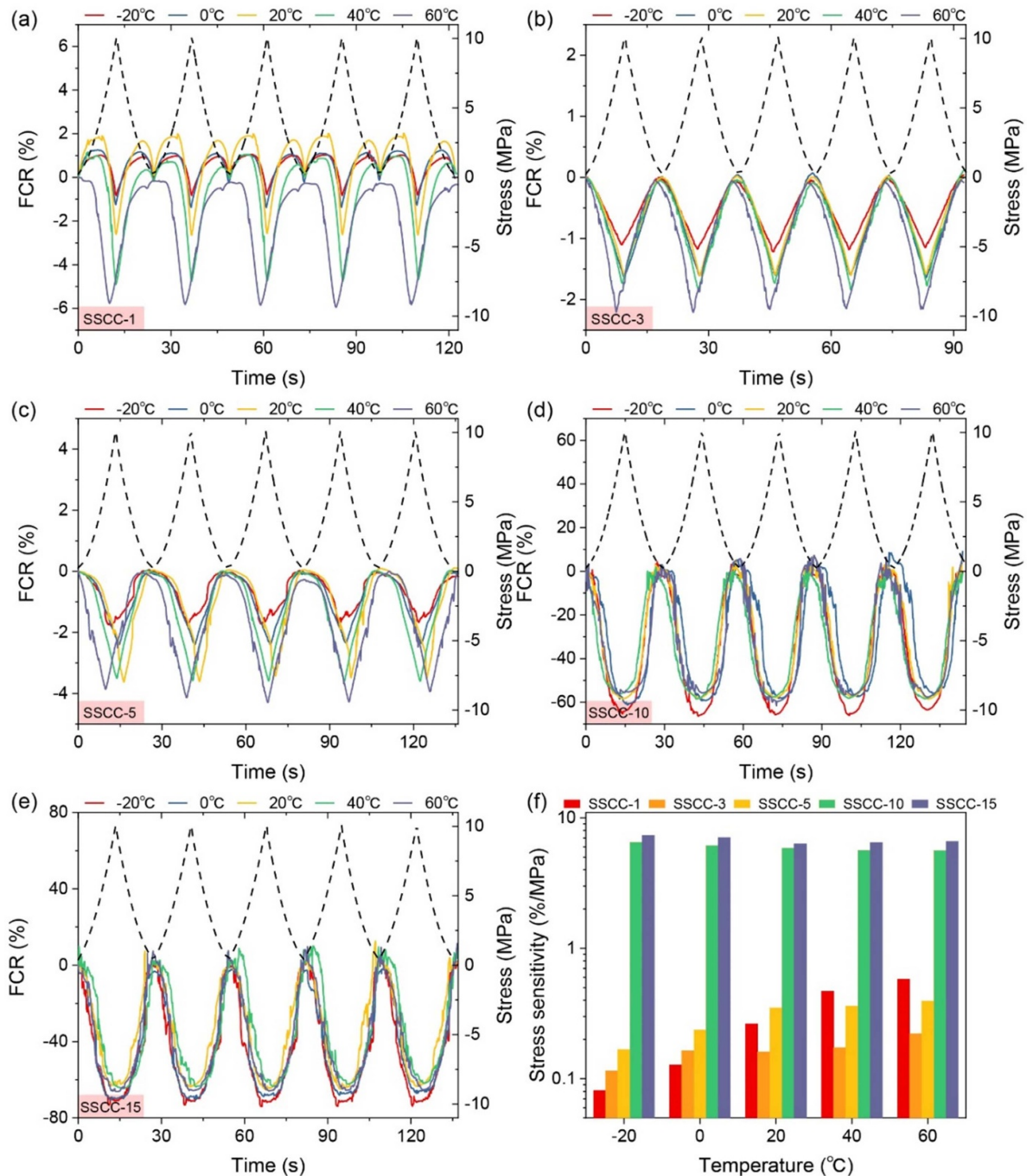


**Figure 9.** Temperature-sensitive property of SSCC-15 during four heating–cooling cycles.

**Figure 10.** Self-sensing behaviors of SSCCs with CNT/NCB composite fillers under different temperatures. (a) SSCC-1. (b) SSCC-3. (c) SSCC-5. (d) SSCC-10. (e) SSCC-15. (f) Stress sensitivity of SSCCs versus temperature.

*3.2. Temperature effect on piezoresistive property of SSCCs with CNT/NCB*

Since plain SSCC has little or no self-sensing property, the case of the specimen SSCC-0 is not taken into account in this section. Figure 10 shows the FCR variations of the SSCCs under five cyclic uniaxial compressions at temperatures of $-20\,^{\circ}\mathrm{C}$, $0\,^{\circ}\mathrm{C}$, $20\,^{\circ}\mathrm{C}$, $40\,^{\circ}\mathrm{C}$, and $60\,^{\circ}\mathrm{C}$, respectively. It is clear that all the SSCC specimens demonstrate a good piezoresistive property at the considered temperatures with reversible

FCR variations upon loading and unloading, indicating no microstructure degradation of the SSCCs over the temperature range of concern [56]. However, the FCR amplitude is affected by temperature variation and filler content. The stress sensitivity ($|\mathrm{FCR}|/\sigma$, here $\sigma$ is the amplitude of applied stress) of each SSCC specimen is shown in figure 10(f). In general, the stress sensitivity of the SSCCs shows an increasing trend with the increase of filler content. The maximum enhancement of the stress sensitivity is observed at $-20\,^{\circ}\mathrm{C}$, from $0.08\%\,\mathrm{MPa}^{-1}$ for the specimen SSCC-1 to $7.33\%\,\mathrm{MPa}^{-1}$ for the speci-
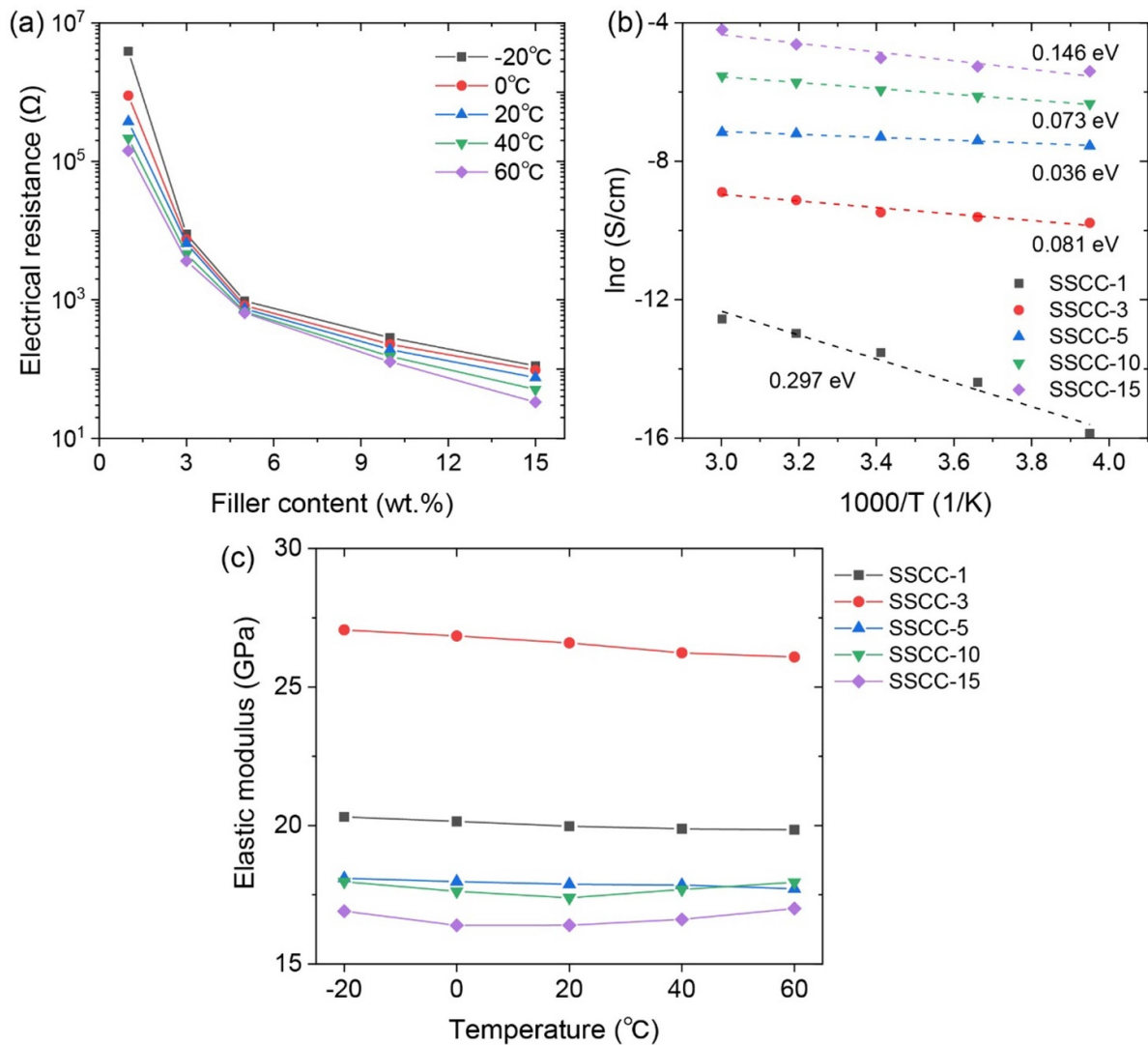
**Figure 11.** (a) Electrical resistance of SSCCs as a function of filler content under different temperatures, at 10 MPa. (b) Arrhenius plots of electrical conductivity versus reciprocal absolute temperature for SSCCs, at 10 MPa. (c) Elastic modulus of SSCCs as a function of temperature.

men SSCC-15 (nearly 100 times higher). However, when the temperature is above 20 °C, the stress sensitivity has its lowest value at the filler content of 3.0 wt% (the specimen SSCC-3), and afterwards the stress sensitivity exhibits a large rise with increasing filler content. For a given filler content, the stress sensitivity of the SSCCs shows an upward trend with the temperature growth when the filler content is lower than 5.0 wt%, while it declines slightly when the filler content is 10.0 wt% (the specimen SSCC-10) and 15.0 wt% (the specimen SSCC-15). The results indicate that the stress sensitivity is affected by temperature in different patterns in accordance with filler contents, and thus the temperature effect is filler concentration-dependent.

To discover the mechanism as to how the temperature affects the piezoresistive property of the SSCCs, the percolation plots and Arrhenius plots of the SSCCs under 10 MPa compression are illustrated in figure 11, which can be compared with the results given in figure 4.

As shown in figure 11(a), the percolation phenomenon takes place when the filler content is above 1.0 wt% regardless of what the temperature is, which is the same as shown in figure 4(d). In addition, as shown in figure 11(b), the Arrhenius plots of the electrical conductivity versus the reciprocal of absolute temperature for the SSCCs at 10 MPa are quite similar to those in figure 4(b). However, the $E_a$ values of the SSCCs at 10 MPa are different from those obtained from figure 4(b). These results indicate that under the simultaneous excitations of temperature and loading, the overall distribution of conductive network in the SSCCs remains unchanged, thereby the repeatability of the SSCCs is not affected. However, under dynamic compression, tunneling distances and contact resistances among conductive fillers are dynamically changed. In addition, the stiffness of the SSCCs varies under different temperatures due to the temperature sensitivity of the mechanical properties and the phase transformations of the constituents in the SSCCs [57].

Figure 11(c) shows the elastic modulus of the SSCCs as a function of temperature. The trends show that the elastic modulus of the specimens SSCC-1, SSCC-3 and SSCC-5 decreases in $-20\,^\circ$C to $60\,^\circ$C temperature range, which is the same as reported for the plain concrete [58]. However, in the case of the specimen SSCC-10, the elastic modulus decreases at temperatures between $-20\,^\circ$C and $20\,^\circ$C, and afterwards it turns to increase with increasing temperature. The transition temperature is even reduced to $0\,^\circ$C for the specimen SSCC-15, indicating that the addition of CNT/NCB composite filler may prevent the elastic modulus from a gradual reduction at the range of $-20\,^\circ$C to $60\,^\circ$C due to the bridging effect of CNTs [58, 59]. The temperature-dependent stiffness associated with the temperature-activated motion of charge carriers changes the connectivity of conductive network in the SSCCs (different $E_a$ values) at different temperatures, thus demonstrating different stress sensitivities. For the specimens SSCC-1, SSCC-3 and SSCC-5 where the conductive network is on the point of establishment and the tunneling conduction plays a dominant role as discussed in section 3.1, the stress sensitivity is highly susceptible to temperature variation and increases with increasing temperature. With the increase of filler content, the stress sensitivity is in general increased while the temperature effect is reduced since the contact conduction dominates and the formation of conductive network is insensitive to temperature variation. As a result, the stress sensitivity decreases slightly upon temperature rise when the filler content is high.

### 3.3. Extraction of temperature-induced resistance using Bayesian BSS method

Based on the above discussion, the effect of temperature on the piezoresistive property of SSCCs is highly related to their temperature-sensitive property, which is quite complicated and inevitable. Even though a high level of filler doping can reduce the temperature effect to a certain extent, this undesirable effect is an obstacle to the practical application of SSCCs. To extract the temperature-induced resistance variation from the mixed response of SSCCs, a Bayesian BSS method with Gaussian process (GP) prior is developed to extract the thermal response in this section.

#### 3.3.1. Bayesian BSS method.
BSS is a powerful signal processing tool for identifying individual ingredients from mixed signals. The unknown individual ingredients and their contributions to the resulting mixtures are defined in terms of sources and a mixing matrix. Generally, the BSS problem in the time domain can be written as [60]:

$$\mathbf{X}(t) = \mathbf{Y}(t) + \mathbf{Z}(t) = \mathbf{A}\mathbf{S}(t) + \mathbf{Z}(t) \tag{4}$$

where $\mathbf{X}(t)$ is a vector of observation signals collected by different sensors, which comprises a vector of pure observation signals $\mathbf{Y}(t)$ and a noise vector $\mathbf{Z}(t)$. $\mathbf{S}(t)$ is a vector of underlying sources mixed in the observation signals and $\mathbf{A}$ is the mixing matrix.

To determine the unknown $\mathbf{S}(t)$ and $\mathbf{A}$, the independent component analysis and the second-order blind identification methods have mostly been used [40, 61, 62]. However, these two traditional methods for solving the BSS problem have difficulties in dealing with underdetermined mixtures in which the number of observations is less than the number of sources. In addition, the noise sequences from different sensors are assumed to be independent and identically distributed Gaussian random variables all with the same variance. Different noise levels among different sensors are not fully accounted for in these methods. Since each individual SSCC has specific performance because of the heterogeneity of cement-based matrix and uncertainties brought in the installation, different noise levels are unavoidable in reality. In this study, a Bayesian BSS method is pursued to address the uncertainty and underdetermination in BSS problems. In this connection, a diagonal covariance matrix $\sum_Z$ is introduced to express different noise levels as

$$p\left(\mathbf{Z}\middle|\sum{}_Z\right) = \prod_{t=1}^{L}\mathcal{N}\left(\mathbf{Z}(t);0,\sum{}_Z\right) \tag{5}$$

where $L$ is the time length and $\mathcal{N}(\mathbf{Z}(t);0,\sum_Z)$ implies that $\mathbf{Z}(t)$ obeys a normal distribution with zero mean and a variance $\sum_Z$, in which the $i$th diagonal element denotes the noise power $\sigma_i^2$ at the $i$th sensor. With this consideration, the likelihood function of the observation matrix $\mathbf{X}$ can be given as

$$p\left(\mathbf{X}\middle|\mathbf{A},\mathbf{S},\sum{}_Z\right) = \prod_{t=1}^{L}p\left(\mathbf{X}(t)\middle|\mathbf{A},\mathbf{S}(t),\sum{}_Z\right)$$
$$= \prod_{t=1}^{L}\mathcal{N}\left(\mathbf{X}(t);\mathbf{A}\mathbf{S}(t),\sum{}_Z\right). \tag{6}$$

To exploit the temporal structure of sources in the context of Bayesian inference, the GP is introduced to define the prior distribution of the unknown sources. In this model, the prior mean function is fixed to zero and the covariance function adopts the well-known squared-exponential (SE) kernel function [63]. Thus, the source prior can be expressed as

$$p(\mathbf{S}|K_j) = \prod_{j=1}^{n}p(\mathbf{S}_j^{\mathrm{T}}) = \prod_{j=1}^{n}\mathrm{GP}(\mathbf{S}_j^{\mathrm{T}};0,K_j) \tag{7}$$

where $\mathbf{S}_j$ is the $j$th source signal and $K_j$ is the covariance matrix in the form of an SE kernel function of two time instants $t$ and $t'$,

$$K_j(t,t') = \partial \times \exp\left(-\frac{|t-t'|^2}{2h_j^2}\right) \tag{8}$$

where $\partial$ is a scale factor of the SE kernel to indicate the power of the generated GP and $h_j$ is the characteristic length-scale of the $j$th source signal that controls the signal smoothness, which can be determined automatically by defining it as a hyperparameter in implementing the Bayesian inference.
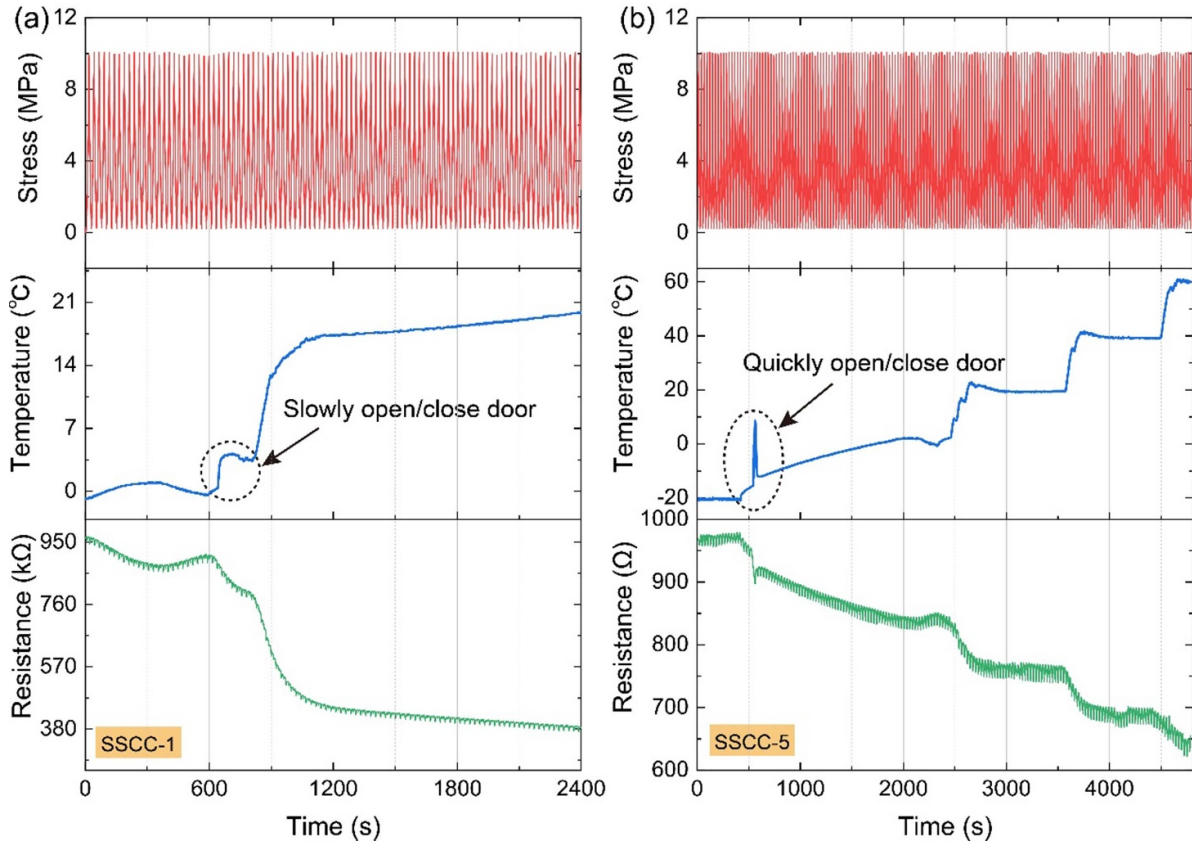
**Figure 12.** Raw responses of (a) SSCC-1 and (b) SSCC-5 and their separated components of temperature and dynamic loading variations.

To establish a model with discriminative inferences for different sensors, the prior distribution of the mixing matrix **A** is specified as

$$p\left(\mathbf{S}|\theta\right)=\prod_{i=1}^{m}\prod_{j=1}^{n}p\left(a_{ij}\right)=\prod_{i=1}^{m}\prod_{j=1}^{n}\mathcal{N}\left(a_{ij};0,\theta_{ij}\right) \quad (9)$$

where $a_{ij}$ is an element of the mixing matrix, $\theta_{ij}$ is the variance of $a_{ij}$ and can be considered as a hyperparameter of the mixing matrix prior.

Being a commonly used conjugate prior distribution in line with Gaussian likelihood, the inverse-gamma (IG) distribution is used as the prior distribution of the variances of the noise matrix $\sum_Z$ and the mixing matrix $\theta$,

$$p\left(\Sigma_Z\right)=\prod_{j=1}^{m}p\left(\Sigma_{Z_{ii}}|\alpha_Z,\beta_Z\right)=\prod_{t=1}^{m}\text{IG}\left(\sigma_i^2|\alpha_Z,\beta_Z\right) \quad (10)$$

$$p\left(\theta\right)=\prod_{i=1}^{m}\prod_{j=1}^{n}p\left(\theta_{ij}|\alpha_a,\beta_a\right)=\prod_{i=1}^{m}\prod_{j=1}^{n}\text{IG}\left(\theta_{ij}|\alpha_a,\beta_a\right) \quad (11)$$

where $\alpha_Z,\beta_Z,\ \alpha_a$ and $\beta_a$ are hyperparameters of the IG distribution.

Due to the non-negativity of the characteristic length-scale ($h_j$) of the $j$th source signal, the gamma distribu-

tion is employed to describe the source hyperparameter feature,

$$p\left(h\right)=\prod_{j=1}^{n}p\left(h_j\right)=\prod_{j=1}^{n}\text{G}\left(h_j|\alpha_s,\beta_s\right) \quad (12)$$

where $\alpha_s$ and $\beta_s$ are given parameters.

Finally, the joint posterior distribution of the sources, mixing matrix, and noise can be obtained by Bayes' theorem as,

$$\begin{aligned}
&p\left(\mathbf{A},\mathbf{S},\Sigma_Z,h,\theta|\mathbf{X}\right)\\
&\propto p\left(\mathbf{X}|\mathbf{A},\mathbf{S},\Sigma_Z\right)\times p\left(\mathbf{A}|\theta\right)\times p\left(\theta\right)\times p\left(h\right)\times p\left(\Sigma_Z\right)\\
&=\prod_{t=1}^{L}\mathcal{N}\left(\mathbf{X}\left(t\right);\mathbf{AS}\left(t\right),\sum\nolimits_Z\right)\times\prod_{j=1}^{n}\text{GP}\left(\mathbf{S}_j^{\text{T}};0,K_j\right)\\
&\quad\times\prod_{i=1}^{m}\prod_{j=1}^{n}\mathcal{N}\left(a_{ij};0,\theta_{ij}\right)\times\prod_{i=1}^{m}\prod_{j=1}^{n}\text{IG}\left(\theta_{ij}|\alpha_a,\beta_a\right)\\
&\quad\times\prod_{j=1}^{n}\text{G}\left(h_j|\alpha_s,\beta_s\right)\times\prod_{t=1}^{m}\text{IG}\left(\sigma_i^2|\alpha_Z,\beta_Z\right). \quad (13)
\end{aligned}$$

With the expression of the joint posterior distribution given in equation (13), a refined Markov chain Monto Carlo algorithm, termed the Gibbs-within-metropolis algorithm is used to numerically compute the probabilistic characteristics of the sources, mixing matrix and noise. The detailed algorithmic
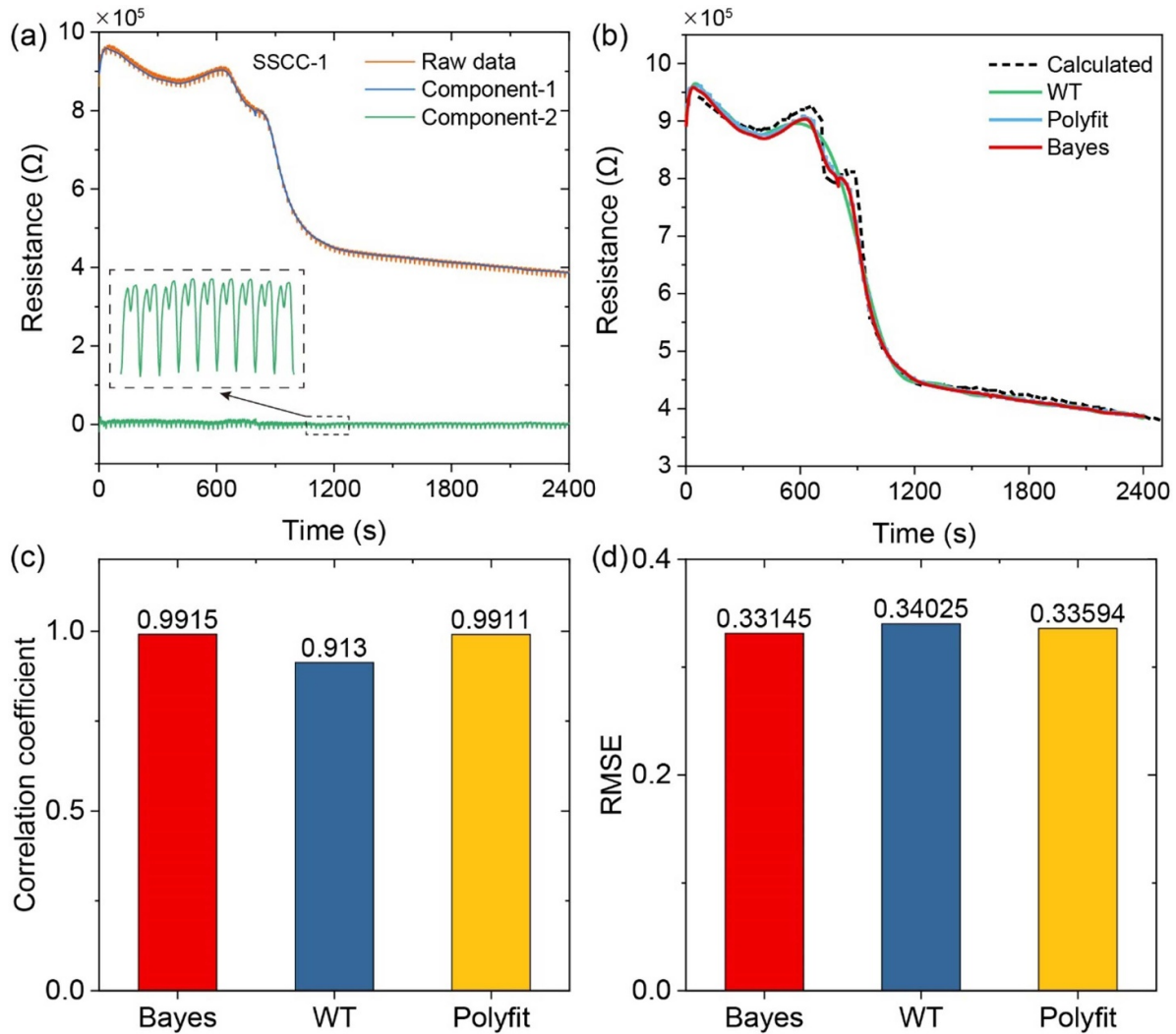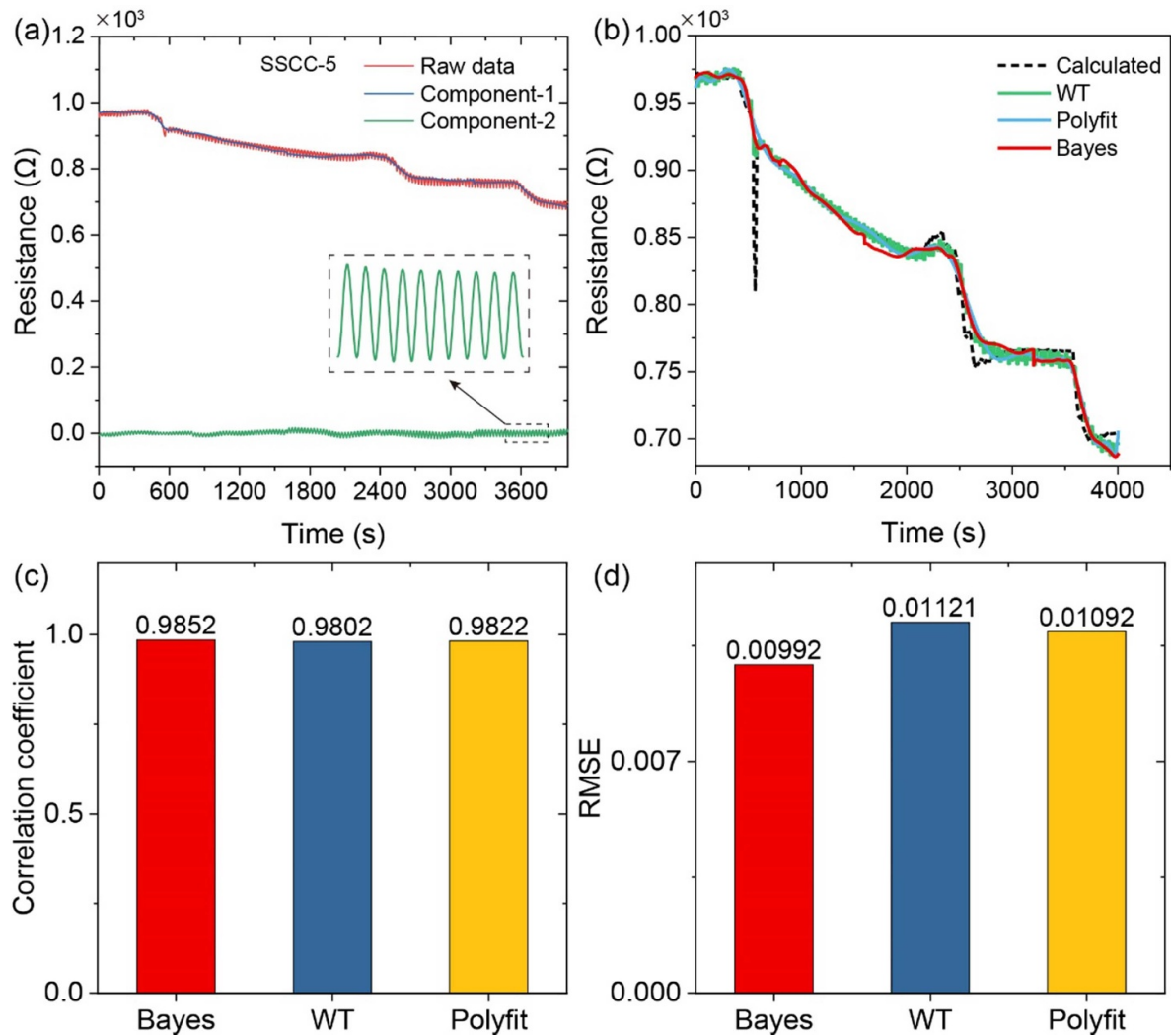
**Figure 13.** Separation result of SSCC-1. (a) Two components separated by Bayesian BSS. (b) Comparison of component-1 extracted by Bayesian BSS (Bayes), wavelet transformation (WT) and polyfit methods with its calculated values. (c) CC. (d) RMSE.

procedures can be found in our previous work [44]. A computer program of the proposed Bayesian BSS method has been developed using MATLAB® language.

*3.3.2. Experimental verification.* To examine the effectiveness of the proposed Bayesian BSS method, experimental tests were carried out under the environment of both temperature (source-1) and loading (source-2) variations. For brevity, only the specimen SSCC-1 that has the highest temperature sensitivity and the specimen SSCC-5 that has the lowest temperature sensitivity are demonstrated. During the tests, the temperature variation was controlled by using the environmental chamber and manually opening/closing the door of the chamber to simulate different temperature-varying manners. In the meantime, the specimens were dynamically compressed with a force amplitude of 10 MPa and a constant loading rate of 0.6 mm min$^{-1}$. Figure 12 shows the electrical resistance variations of the specimens SSCC-1 and SSCC-5 under simultaneous excitations of time-varying temperature and loading.

It is apparent that the response of the SSCCs is a combination of the two excitations in which dynamic loading produces a series of weak resistance variation peaks and temperature variation generates a significant alteration in the resistance. The total variation trend keeps pace with temperature variation. For instance, a short- or long-time door opening generates perfectly synchronous resistance variation as illustrated in figure 12, which indicates that the temperature of the SSCCs has greater influence on their initial electrical resistance than on the piezoresistive property. Thus, the resistance change due to temperature variation could cause a major problem in implementing the SSCC-based sensors in practice for long-term damage detection and health monitoring. The response signal change due to operational and environmental variations should be separated from the response signal change caused by structural behavior alteration.

The raw response data are then decomposed into two components: (a) component-1 that is due to the excitation of source-1, i.e. temperature; and (b) component-2 that corresponds to the excitation of source-2, i.e. loading, by using the

**Figure 14.** Separation result of SSCC-5. (a) Two components separated by Bayesian BSS. (b) Comparison of component-1 extracted by Bayesian BSS, WT and polyfit methods with its calculated values. (c) CC. (d) RMSE.

proposed Bayesian BSS method. The separation results for the specimens SSCC-1 and SSCC-5 are shown in figures 13 and 14, respectively. In both cases, the Bayesian BSS method achieves satisfactory results in that the temperature-induced resistance change and the loading-induced resistance change are well extracted and reconstructed. The insets in figures 13 and 14 are the enlarged views of the extracted component-2 representing the 'pure' loading-induced resistance change. Repeatable stress sensing response can be observed with no temperature-induced resistance drifts over time. Correlation coefficients (CCs) and root mean square errors (RMSEs) are obtained to evaluate the effectiveness of the proposed method. The CC values are 99.15% for the specimen SSCC-1 and 95.82% for the specimen SSCC-3. The RMSE values are found to be $3.314 \times 10^4$ $\Omega$ and 9.92 $\Omega$ for the specimens SSCC-1 and SSCC-3, respectively, which indicate an excellent performance of the proposed Bayesian BSS for the extraction of temperature-induced responses from the mixed responses of the SSCCs.

For comparison, two built-in algorithms in MATLAB® including the WT and polyfit methods are also applied to extract the temperature-induced resistance change, and the results from the three methods are compared with those calculated using the measured temperatures and the curve fitting equations given in figures 5 and 7. Here, 4-order WT and 20-order polyfit are used due to their good performance after numerous attempts. As shown in figures 13(b) and 14(b), the extracted signals match well with the calculated signals, indicating that both the WT and polyfit methods can effectively extract the temperature-induced excitations. However, compared with the Bayesian BSS method, the lower CC values and higher RMSE values between the extracted values by the WT and polyfit methods and the calculated values demonstrate their relatively poor performance in the extraction of temperature-induced excitations. In addition, it is workload-intensive to adjust the order in the WT and polyfit methods with the attempt to achieve favorable extraction performance. In contrast, the proposed Bayesian BSS method is

self-learning and self-adjusting with higher accuracy, higher robustness and faster computational speed.

It is disappointing that all the three methods are unable to recognize the actions of slowly and quickly opening/closing the chamber door. In addition, the temperature effect on the piezoresistive property of SSCCs discussed in section 3.2 still exists after source separation, which is manifested as time-varying amplitudes of the resistance variation (namely FCR) in component-2. As this effect is attributed to the inherent features of SSCCs, it might be quite difficult to eliminate such effect by the signal post-processing. In addition, as discussed in section 3.2, the piezoresistive sensitivity of SSCCs is mainly temperature-dependent, which means that the loading-induced response and the temperature-induced response are closely related. However, it is assumed that the sources to be separated are exactly independent in the proposed Bayesian BSS method. Therefore, this method is difficult to remove temperature effect on the piezoresistive sensitivity of SSCCs unless a time-varying mixing matrix that describes the relationship between temperature and sensitivity is considered.

## 4. Conclusions

In this paper, the electrical and piezoresistive properties of SSCCs reinforced with electrostatic self-assembled CNT/NCB composite fillers under different temperature conditions were explored systematically. Upon temperature variation, the SSCCs exhibit a noticeable NTC effect and excellent temperature-sensitive repeatability. However, the temperature-sensitive property of the SSCCs depends on filler content, which is attributed to different electrical conduction mechanisms dominating at different filler contents. Increasing CNT/NCB composite filler can decrease the activation energy of the SSCCs and facilitate the transport of the charge carriers, thus attenuating temperature-sensitivity. Since temperature-dependent stiffness associated with the temperature-activated motion of charge carriers alters the connectivity of conductive network in the SSCCs at different temperatures, temperature has a strong effect on the piezoresistive sensitivity of the SSCCs but no effect on the repeatability.

To eliminate the variation in resistance due to the temperature-sensitive property of the SSCCs, a Bayesian BSS method adopting GP prior was proposed and implemented. Compared to the WT and polyfit methods, the proposed Bayesian BSS method has better performance in terms of both accuracy and computational cost on the extraction of temperature-induced resistance variation. However, it is unable to remove the temperature effect on the piezoresistive sensitivity of the SSCCs. More work regarding the underlying physics of temperature-dependent behaviors of the SSCCs and signal post-processing techniques is needed to realize the practical application of SSCCs.

## Data availability statement

The data that support the findings of this study are available upon reasonable request from the authors.

## Acknowledgments

## ORCID iDs

Siqi Ding ⓘ https://orcid.org/0000-0002-7565-4549
Yi-Qing Ni ⓘ https://orcid.org/0000-0003-1527-7777
Baoguo Han ⓘ https://orcid.org/0000-0002-7081-3221

## References

[1] Ni Y Q, Xia Y, Liao W Y and Ko J M 2009 Technology innovation in developing the structural health monitoring system for Guangzhou New TV Tower *Struct. Control Health Monit.* **16** 73–98

[2] Han B, Yu X and Ou J 2014 *Self-Sensing Concrete in Smart Structures* (Amsterdam: Elsevier)

[3] Das S and Saha P 2018 A review of some advanced sensors used for health diagnosis of civil engineering structures *Measurement* **129** 68–90

[4] Carden E P and Fanning P 2004 Vibration based condition monitoring: a review *Struct. Health Monit.* **3** 355–77

[5] Doebling S W, Farrar C R and Prime M B 1998 A summary review of vibration-based damage identification methods *Shock Vib. Dig.* **30** 91–105

[6] Hong W, Zhang J, Wu G and Wu Z 2015 Comprehensive comparison of macro-strain mode and displacement mode based on different sensing technologies *Mech. Syst. Signal Process.* **50–51** 563–79

[7] Li Y Y 2010 Hypersensitivity of strain-based indicators for structural damage identification: a review *Mech. Syst. Signal Process.* **24** 653–64

[8] Feng D and Feng M Q 2017 Experimental validation of cost-effective vision-based structural health monitoring *Mech. Syst. Signal Process.* **88** 199–211

[9] Majumder M, Gangopadhyay T K, Chakraborty A K, Dasgupta K and Bhattacharya D K 2008 Fibre Bragg gratings in structural health monitoring–present status and applications *Sens. Actuators* A **147** 150–64

[10] Taheri S 2019 A review on five key sensors for monitoring of concrete structures *Constr. Build. Mater.* **204** 492–509

[11] Han B, Ding S and Yu X 2015 Intrinsic self-sensing concrete and structures: a review *Measurement* **59** 110–28

[12] Han W, Zhao G, Zhang X, Zhou S, Wang P, An Y and Xu B 2015 Graphene oxide grafted carbon fiber reinforced siliconborocarbonitride ceramics with enhanced thermal stability *Carbon* **95** 157–65

[13] Li G Y, Wang P M and Zhao X 2007 Pressure-sensitive properties and microstructure of carbon nanotube reinforced cement composites *Cem. Concr. Compos.* **29** 377–82

[14] Howser R N, Dhonde H B and Mo Y L 2011 Self-sensing of carbon nanofiber concrete columns subjected to reversed cyclic loading *Smart Mater. Struct.* **20** 085031

[15] Han B G, Han B Z and Ou J P 2009 Experimental study on use of nickel powder-filled portland cement-based composite for fabrication of piezoresistive sensors with high sensitivity *Sens. Actuators* A **149** 51–5

[16] Sun S, Ding S, Han B, Dong S, Yu X, Zhou D and Ou J 2017 Multi-layer graphene-engineered cementitious composites with multifunctionality/intelligence *Composites* B **129** 221–32

[17] D'Alessandro A, Rallini M, Ubertini F, Materazzi A L and Kenny J M 2016 Investigations on scalable fabrication procedures for self-sensing carbon nanotube cement-matrix composites for SHM applications *Cem. Concr. Compos.* **65** 200–13

[18] Song C and Choi S 2017 Moisture-dependent piezoresistive responses of CNT-embedded cementitious composites *Compos. Struct.* **170** 103–10

[19] Han B, Zhang L, Zeng S, Dong S, Yu X, Yang R and Ou J 2017 Nano-core effect in nano-engineered cementitious composites *Composites* A **95** 100–9

[20] Materazzi A L, Ubertini F and D'Alessandro A 2013 Carbon nanotube cement-based transducers for dynamic sensing of strain *Cem. Concr. Compos.* **37** 2–11

[21] García-Macías E, D'Alessandro A, Castro-Triguero R, Pérez-Mira D and Ubertini F 2017 Micromechanics modeling of the electrical conductivity of carbon nanotube cement-matrix composites *Composites* B **108** 451–69

[22] Liu Q, Gao R, Tam V W Y, Li W and Xiao J 2018 Strain monitoring for a bending concrete beam by using piezoresistive cement-based sensors *Constr. Build. Mater.* **167** 338–47

[23] Gupta S, Gonzalez J G and Loh K J 2017 Self-sensing concrete enabled by nano-engineered cement-aggregate interfaces *Struct. Health Monit.* **16** 309–23

[24] García-Macías E and Ubertini F 2019 Earthquake-induced damage detection and localization in masonry structures using smart bricks and kriging strain reconstruction: a numerical study *Earthq. Eng. Struct. Dyn.* **48** 548–69

[25] Ding S, Wang Y W, Ni Y Q and Han B 2020 Structural modal identification and health monitoring of building structures using self-sensing cementitious composites *Smart Mater. Struct.* **29** 055013

[26] Han B, Yu X and Kwon E 2009 A self-sensing carbon nanotube/cement composite for traffic monitoring *Nanotechnology* **20** 445501

[27] Chang C, Song G, Gao D and Mo Y L 2013 Temperature and mixing effects on electrical resistivity of carbon fiber enhanced concrete *Smart Mater. Struct.* **22** 035021

[28] Teomete E 2016 The effect of temperature and moisture on electrical resistance, strain sensitivity and crack sensitivity of steel fiber reinforced smart cement composite *Smart Mater. Struct.* **25** 075024

[29] Han B, Zhang L and Ou J 2017 *Smart and Multifunctional Concrete toward Sustainable Infrastructures* (Berlin: Springer)

[30] Ding S, Dong S, Ashour A and Han B 2019 Development of sensing concrete: principles, properties and its applications *J. Appl. Phys.* **126** 241101

[31] Wen S, Wang S and Chung D D L 1999 Carbon fiber structural composites as thermistors *Sens. Actuators* A **78** 180–8

[32] Han B, Zhang L, Sun S, Yu X, Dong X, Wu T and Ou J 2015 Electrostatic self-assembly carbon nanotube/nano carbon black composite fillers reinforced cement-based materials with multifunctionality *Composites* A **79** 103–15

[33] Kim G M, Park S M, Ryu G U and Lee H K 2017 Electrical characteristics of hierarchical conductive pathways in cementitious composites incorporating CNT and carbon fiber *Cem. Concr. Compos.* **82** 165–75

[34] Wang H, Zhang A, Zhang L, Wang Q, Yang X H, Gao X and Shi F 2020 Electrical and piezoresistive properties of carbon nanofiber cement mortar under different temperatures and water contents *Constr. Build. Mater.* **265** 120740

[35] Han B, Ding S, Wang J and Ou J 2019 *Nano-Engineered Cementitious Composites: Principles and Practices* (Berlin: Springer)

[36] Monteiro A O, Loredo A, Costa P M F J, Oeser M and Cachim P B 2017 A pressure-sensitive carbon black cement composite for traffic monitoring *Constr. Build. Mater.* **154** 1079–86

[37] Ou J and Han B 2009 Piezoresistive cement-based strain sensors and self-sensing concrete components *J. Intell. Mater. Syst. Struct.* **20** 329–36

[38] Al-Dahawi A, Sarwary M H, Öztürk O, Yıldırım G, Akın A, Şahmaran M and Lachemi M 2016 Electrical percolation threshold of cementitious composites possessing self-sensing functionality incorporating different carbon-based materials *Smart Mater. Struct.* **25** 105005

[39] Ko J M and Ni Y Q 2005 Technology developments in structural health monitoring of large-scale bridges *Eng. Struct.* **27** 1715–25

[40] Zhu Y, Ni Y Q, Jesus A, Liu J and Laory I 2018 Thermal strain extraction methodologies for bridge structural condition assessment *Smart Mater. Struct.* **27** 105051

[41] Bastani A, Amindavar H, Shamshirsaz M and Sepehry N 2012 Identification of temperature variation and vibration disturbance in impedance-based structural health monitoring using piezoelectric sensor array method *Struct. Health Monit.* **11** 305–14

[42] Lim H J, Kim M K, Sohn H and Park C Y 2011 Impedance based damage detection under varying temperature and loading conditions *NDT & E Int.* **44** 740–50

[43] Oh C K and Sohn H 2009 Damage diagnosis under environmental and operational variations using unsupervised support vector machine *J. Sound Vib.* **325** 224–39

[44] Xu C and Ni Y Q 2018 A Bayesian source separation method for noisy observations by embedding Gaussian process prior *7th World Conf. Struct. Control Monit.* (*Qingdao, China*)

[45] Liu X Z, Xu C and Ni Y Q 2019 Wayside detection of wheel minor defects in high-speed trains by a Bayesian blind source separation method *Sensors* **19** 3981

[46] Han B, Wang Y, Ding S, Yu X, Zhang L, Li Z and Ou J 2017 Self-sensing cementitious composites incorporated with botryoid hybrid nano-carbon materials for smart infrastructures *J. Intell. Mater. Syst. Struct.* **28** 699–727

[47] Ding S, Ruan Y, Yu X, Han B and Ni Y Q 2019 Self-monitoring of smart concrete column incorporating CNT/NCB composite fillers modified cementitious sensors *Constr. Build. Mater.* **201** 127–37

[48] Jennings H M, Thomas J J, Gevrenov J S, Constantinides G and Ulm F J 2007 A multi-technique investigation of the nanoporosity of cement paste *Cem. Concr. Res.* **37** 329–36

[49] Feteira A 2009 Negative temperature coefficient resistance (NTCR) ceramic thermistors: an industrial perspective *J. Am. Ceram. Soc.* **92** 967–83

[50] Tuan C Y and Yehia S 2004 Evaluation of electrically conductive concrete containing carbon products for deicing *ACI Mater. J.* **101** 287–93

[51] McCarter W J, Starrs G, Chrisp T M and Banfill P F G 2007 Activation energy and conduction in carbon fibre reinforced cement matrices *J. Mater. Sci.* **42** 2200–3

[52] Mitoma N, Aikawa S, Ou-Yang W, Gao X, Kizu T, Lin M F, Fujiwara A, Nabatame T and Tsukagoshi K 2015 Dopant selection for control of charge carrier density and mobility in amorphous indium oxide thin-film transistors: comparison between Si- and W-dopants *Appl. Phys. Lett.* **106** 042106

[53] Shen J T, Buschhorn S T, Jtm D H, Schulte K and Fiedler B 2015 Pressure and temperature induced electrical resistance change in nano-carbon/epoxy composites *Compos. Sci. Technol.* **115** 1–8

[54] Nakano H, Shimizu K, Takahashi S, Kono A, Ougizawa T and Horibe H 2012 Resistivity–temperature characteristics of filler-dispersed polymer composites *Polymer* **53** 6112–7

[55] Pane I and Hansen W 2005 Investigation of blended cement hydration by isothermal calorimetry and thermal analysis *Cem. Concr. Res.* **35** 1155–64

[56] Gallucci E, Zhang X and Scrivener K L 2013 Effect of temperature on the microstructure of calcium silicate hydrate (C–S–H) *Cem. Concr. Res.* **53** 185–95

[57] Lee J, Xi Y, Willam K and Jung Y 2009 A multiscale model for modulus of elasticity of concrete at high temperatures *Cem. Concr. Res.* **39** 754–62

[58] Khaliq W and Kodur V 2011 Thermal and mechanical properties of fiber reinforced high performance self-consolidating concrete at elevated temperatures *Cem. Concr. Res.* **41** 1112–22

[59] Zhang L W, Kai M F and Liew K M 2017 Evaluation of microstructure and mechanical performance of CNT-reinforced cementitious composites at elevated temperatures *Composites* A **95** 286–93

[60] Belouchrani A, Abed-Meraim K and Cardoso J-F M E 1997 A blind source separation technique using second-order statistics *IEEE Trans. Signal Process.* **45** 434–44

[61] Delorme A and Eeglab M S 2004 An open source toolbox for analysis of single-trial EEG dynamics including independent component analysis *J. Neurosci. Methods* **134** 9–21

[62] Hyvärinen A 1999 Fast and robust fixed-point algorithms for independent component analysis *IEEE Trans. Neural Netw.* **10** 626–34

[63] Wan H P and Ni Y Q 2019 Bayesian multi-task learning methodology for reconstruction of structural health monitoring data *Struct. Health Monit.* **18** 1282–309